INTERNATIONAL JOURNAL OF OPTIMIZATION IN CIVIL ENGINEERING
Int. J. Optim. Civil Eng., 2026; 16(2):165-184

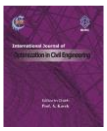

PREDICTION OF NONLINEAR INTER-STORY DRIFTS IN STEEL MOMENT FRAMES UNDER SEISMIC LOADING USING CASCADE FORWARD NEURAL NETWORKS

A.S. Hadi Ajli and S. Gholizadeh[*, †]
Department of Civil Engineering, Urmia University, Urmia, Iran

[DOI: 10.22068/ijoce.2026.16.2.665]

ABSTRACT

This paper aims to predict the maximum inter-story drift ratios of steel moment-resisting frame (MRF) structures under seismic loading, corresponding to different performance levels, using cascade-forward back-propagation (CFBP) neural network models. To this end, CFBP networks with varying numbers of hidden layer neurons are trained on nonlinear time-history analysis results of 6- and 12-story planar steel MRFs subjected to a suite of earthquake ground motions. The predictive performance of the trained models is systematically compared. Numerical results demonstrate that CFBP networks with 15 neurons in the hidden layer consistently outperform other network architectures, yielding more accurate predictions of the maximum inter-story drift ratios at each seismic performance level for both frame heights. These findings highlight the potential of moderately sized CFBP networks as efficient surrogates for nonlinear dynamic analysis in performance-based seismic assessment.

Keywords: nonlinear time history analysis; steel moment resisting frame; performance level; cascade-forward back-propagation; neural network.

Received: 26 January 2026 Accepted: 29 March 2026

1. INTRODUCTION

For any structure to remain functional and safe after an earthquake, it must possess adequate seismic resistance, a requirement that modern design codes now address by embracing performance-based design (PBD) as a central strategy [1]. PBD requires engineers to evaluate the nonlinear inelastic response of structures under seismic loading, typically using nonlinear time-history analysis. While accurate, this approach is computationally demanding

[*]Corresponding author: Department of Civil Engineering, Urmia University, Urmia, P.O. box 165, Iran
[†]E-mail address: s.gholizadeh@urmia.ac.ir (S. Gholizadeh)

and time-consuming, especially when applied to realistic building models. Structural engineers are therefore challenged to design cost-effective and reliable structures that meet performance targets without high computational cost. To address this issue, performance-based design optimization (PBDO) techniques have been developed, and numerous studies have explored their application [2-7]. Among the most promising solutions are metaheuristic algorithms, which are inspired by stochastic natural phenomena (e.g., genetic evolution, swarm behavior) and do not require gradient information, making them relatively simple to implement computationally [8-12]. However, metaheuristic algorithms are population-based search methods. Each optimization iteration requires evaluating many candidate designs, and for PBDO, each evaluation involves a full nonlinear seismic analysis. Consequently, the overall computational burden remains extremely high, often prohibitive for routine practice. This issue has motivated researchers to use surrogate models that can approximate nonlinear time-history responses with much lower computational cost.

Neural networks have emerged as one of the most effective alternatives to reduce this burden. In recent years, there has been growing interest in using artificial intelligence techniques, particularly neural networks, to simplify complex engineering problems. Neural networks are computational models inspired by the structure and function of the human brain. They excel at learning from data and modeling complex nonlinear relationships without explicit physical equations. Their success has been demonstrated across numerous civil engineering domains, including structural health monitoring, material behavior prediction, and seismic response modeling [13-17].

Despite these advances, few studies have systematically examined the ability of cascade-forward back-propagation (CFBP) neural networks, a variant with direct connections from the input layer to both hidden and output layers, to predict maximum inter-story drift ratios of steel moment-resisting frames (MRFs) at different seismic performance levels. Most existing work has focused on simpler network architectures or on predicting only peak global responses (e.g., roof displacement). Moreover, the effect of hidden layer size on prediction accuracy for multi-story steel MRFs under seismic loading has not been thoroughly investigated.

To fill this gap, the present study employs CFBP neural network models with varying numbers of hidden layer neurons to predict the maximum inter-story drift ratios of steel MRFs. Two design examples are considered: a 6-story and a 12-story steel MRF. Networks with 5, 10, 15, and 20 hidden neurons are trained and compared. The results demonstrate that the most accurate predictions are achieved using 15 hidden-layer neurons for both frame heights.

2. SEISMIC RESPONSES AND GROUND MOTION RECORDS

A seismic performance objective defines a target level of structural behavior corresponding to a given earthquake intensity. Establishing such an objective requires specifying two things: the desired structural performance state and the associated seismic hazard level. According to FEMA-356 [1], three standard performance levels are recognized: immediate occupancy (IO), life safety (LS), and collapse prevention (CP). Each of these levels is linked

[DOI: 10.22068/ijoce.2026.16.2.665]

to a specific probability of exceedance over a 50-year period. Specifically, IO corresponds to a 50% exceedance probability, LS to 10%, and CP to 2% in 50 years. In the present study, the acceleration response spectra for these hazard levels are derived from the Iranian seismic design code [18], assuming soil type III and a very high seismicity region. These spectra are illustrated in Fig. 1.

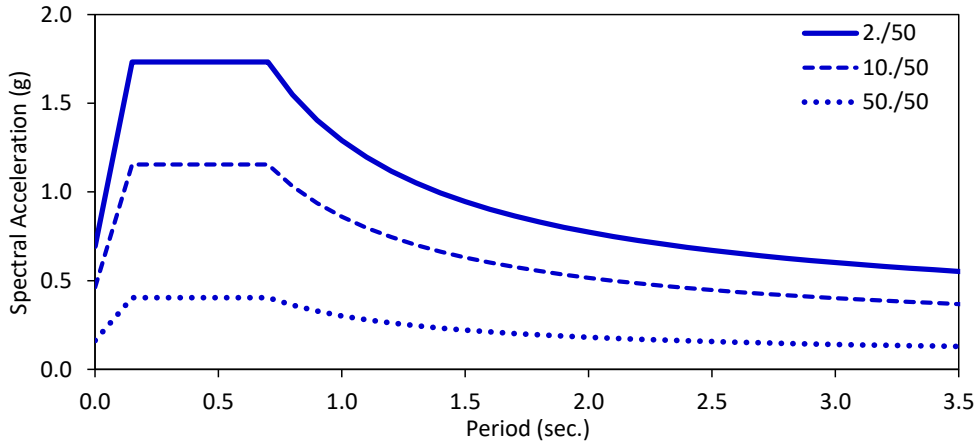

Figure 1: Acceleration response spectra

In seismic performance-based design, it is essential to evaluate structural behavior using nonlinear analysis methods. Accordingly, this paper employs nonlinear time-history analysis conducted through the OpenSees platform [19] to assess the seismic response of the structures under the ground motion records listed in Table 1 (the acceleration time histories of these records are also plotted in Fig. 2). For each record, the peak response quantities are extracted, and the average of these peak values is taken as the representative structural response for each performance level. It is worth noting that this study employs only five ground motion records for demonstration purposes. In principle, a larger set of records could be used without altering the core proposed methodology, as the neural network training framework remains independent of the specific number or selection of input ground motions. Previous studies [20-23] have shown that the seismic design of steel MRFs is primarily governed by maximum inter-story drift ratios, while other design constraints, such as plastic rotations in beams and columns, are typically not active. Based on this finding, the present study focuses exclusively on the maximum inter-story drift ratios at the IO, LS, and CP performance levels as the key seismic response parameters for the steel MRFs.

Table 1: List of earthquake events

Record No.	Name	Year	Magnitude
1	Northridge	1994	6.7
2	Duzce, Turkey	1999	7.1
3	Hector Mine	1999	7.1
4	Imperial Valley	1979	6.5
5	Kobe, Japan	1995	6.9

[DOI: 10.22068/ijoce.2026.16.2.665]

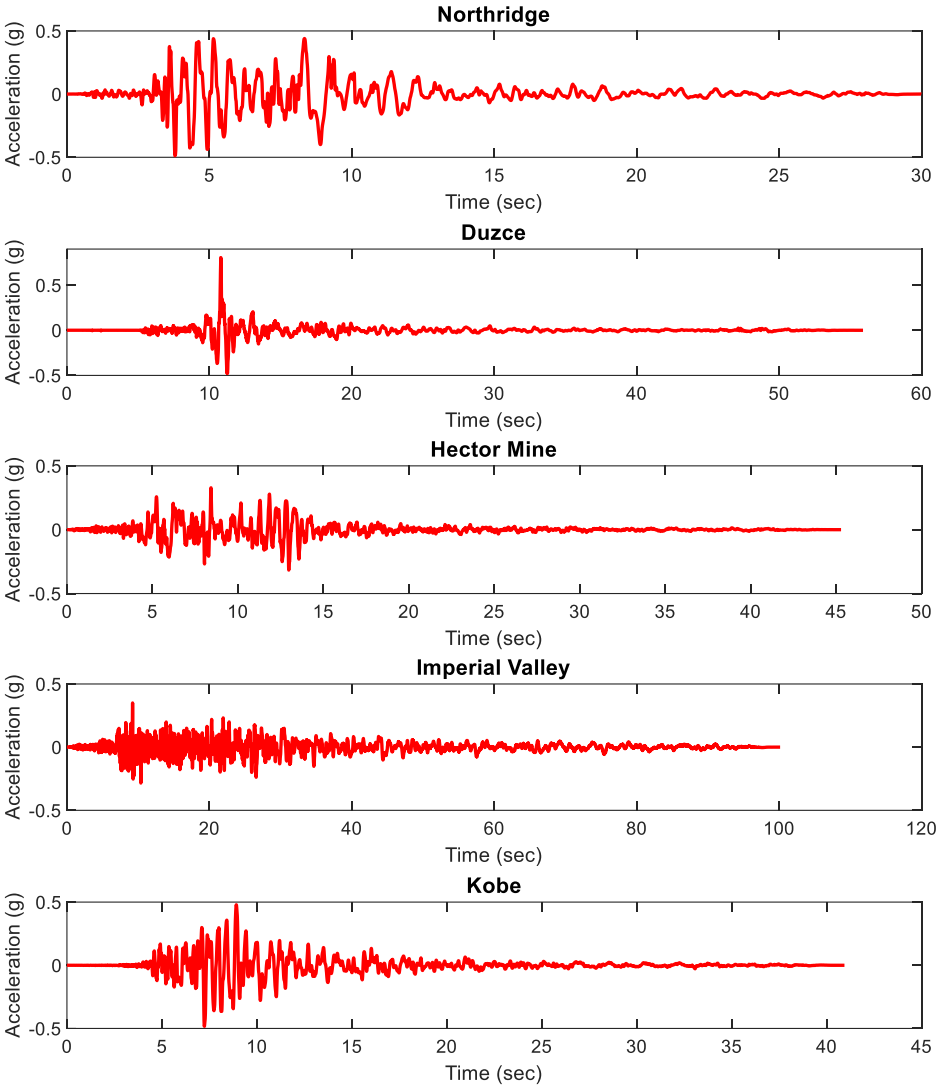

Figure 2: Ground motion records

3. NEURAL NETWORKS

Neural networks serve as highly capable tools for tackling complex, computationally intensive problems. Their popularity stems from the ability to learn from external data and prior experiences, rather than relying solely on explicit rules or physics-based equations. Unlike conventional problem-solving approaches that require predefined formulations of the underlying phenomena, neural networks adapt to new problems by extracting patterns and relationships from past examples. Moreover, their learning is not limited to explicit, desired knowledge; they can also capture implicit information that may not be known to the designer beforehand [24]. This paper employs a cascade-forward multi-layer perceptron trained using the back-propagation algorithm [24]. This neural network architecture is referred to as the

[DOI: 10.22068/ijoce.2026.16.2.665]

cascade-forward back-propagation (CFBP) model, which is schematically shown in Fig. 3.

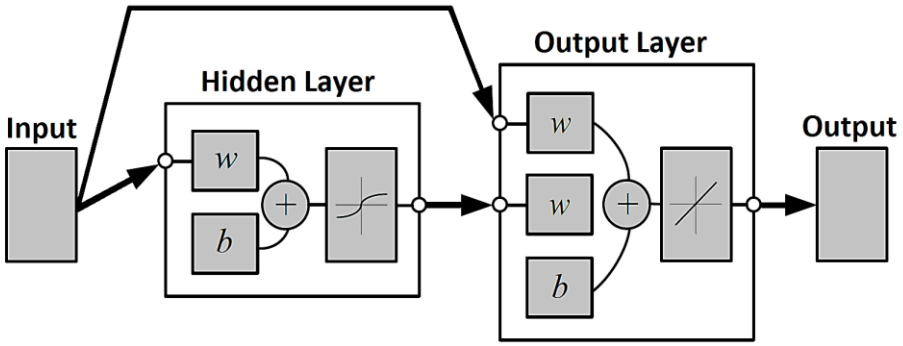

Figure 3: CFBP neural network model

The training algorithm of the CFBP model is a gradient descent optimization algorithm that adjusts the weights in the steepest descent direction according to the following equation:

$$W_{t+1} = W_t - \eta \nabla_t \tag{1}$$

where W_t, ∇_t, and η_t are the weight matrix, the current gradient matrix, and the learning rate, respectively, at iteration t.

The back-propagation technique uses the Levenberg-Marquardt (LM) [24] algorithm to approach second-order training speed without having to compute the Hessian matrix. In the LM algorithm, the updating of the weights is achieved as follows:

$$W_{t+1} = W_t - [J^T J + \alpha I]^{-1} J^T Er \tag{2}$$

where J is the Jacobian matrix, the first derivatives of the network errors to the weights); Er is a vector of network errors; α is a correction factor; and I is the identity matrix.

Regularization is a technique used to prevent overfitting in CFBP models. This is achieved by modifying the performance function of the model through the addition of a term. The added term consists of the mean of the sum of squares of the network weights. This is expressed as [24]:

$$mse_r = \gamma \left(\frac{1}{m} \sum_{k=1}^{m} (Er_k)^2 \right) + \frac{1-\gamma}{nw} \sum_{l=1}^{nw} \left(W_{t,l} \right)^2 \tag{3}$$

where γ and nw are the performance ratio and number of network weights, respectively; m is the size of Er_k.

4. STRUCTURAL MODELS AND METHODOLOGY

In the present work, CFBP models are employed to predict the seismic behavior of planar

[DOI: 10.22068/ijoce.2026.16.2.665]

steel MRFs, considering both 6-story and 12-story configurations. The structural topology and member grouping are depicted in Fig. 4.

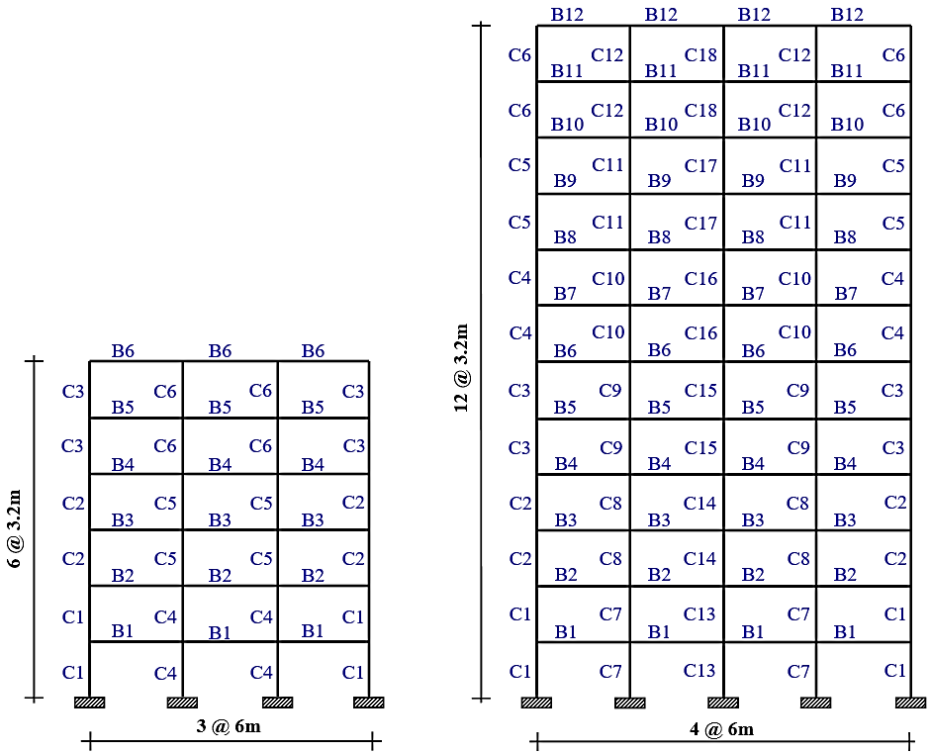

Figure 4: 6- and 12-story steel MRFs

CFBP neural network models are trained to predict the maximum inter-story drift ratios of steel MRFs at different seismic performance levels. For the 6-story and 12-story steel MRFs, the input and output vectors of the neural network models are defined as follows:

6-story frame $$X_6 = \{C1\ \ C2\ \ \ldots C6\ \ B1\ \ B2\ \ \ldots\ \ B6\}^T \quad (4)$$

12-story frame $$X_{12} = \{C1\ \ C2\ \ \ldots C18\ \ B1\ \ B2\ \ \ldots\ \ B12\}^T \quad (5)$$

For 6- and 12-story frames $$Y = \{d_{max}^{IO}\ \ d_{max}^{LS}\ \ d_{max}^{CP}\}^T \quad (6)$$

where X_6 and X_{12} are the input vectors of the NN models for 6 and 12-story steel MRFs, respectively; Y is the output vector; and d_{max}^{IO}, d_{max}^{LS}, and d_{max}^{CP} are the maximum inter-story drift ratios of steel MRFs at IO, LS, and CP performance levels, respectively.

Geometric and strength criteria must be satisfied by every data sample generated for both the 6-story and 12-story steel SMFs. Geometric constraints, in particular, need to be checked at every frame joint. Fig. 5 depicts a typical beam-column joint (one beam connected to two columns), from which the following constraints are derived:

[DOI: 10.22068/ijoce.2026.16.2.665]

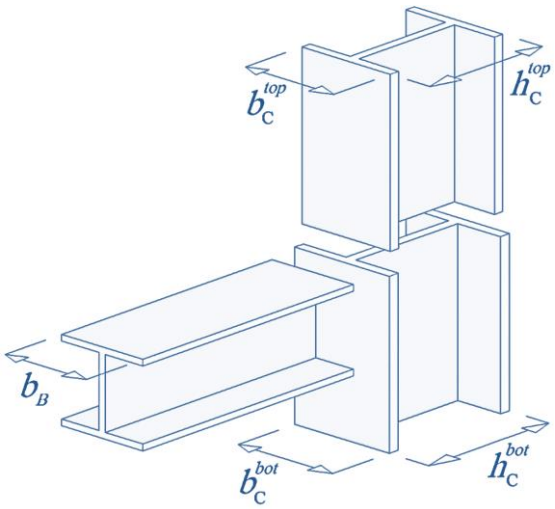

Figure 5: A typical framing joint

$$b_B \leq b_C^{bot}, b_C^{top} \leq b_C^{bot}, h_C^{top} \leq h_C^{bot} \tag{7}$$

The following strength-related constraints apply to each structural element when subjected to non-seismic load combinations [25]:

$$\text{if } \frac{P_u}{\emptyset_c P_n} < 0.2 : \frac{P_u}{2\emptyset_c P_n} + \frac{M_u}{\emptyset_b M_n} \leq 1 \tag{8}$$

$$\text{if } \frac{P_u}{\emptyset_c P_n} \geq 0.2 : \frac{P_u}{\emptyset_c P_n} + \frac{8}{9}\frac{M_u}{\emptyset_b M_n} \leq 1 \tag{9}$$

where P_u is the required axial strength; P_n is the nominal axial strength; $\emptyset_c$ and $\emptyset_b$ are the resistance factors; M_u and M_n are the required and nominal flexural strengths, respectively.

Once a candidate structural design successfully satisfies all the geometric and strength constraints under non-seismic load combinations, it proceeds to seismic performance evaluation. This evaluation consists of performing nonlinear time-history analyses for each scaled ground motion record, listed in Table 1, considering each required seismic performance level (i.e., immediate occupancy, life safety, and collapse prevention). For each record and performance level, the maximum inter-story drift ratios are extracted from the nonlinear time history analysis results. This process is repeated for all structural designs included in the dataset.

The resulting data, comprising input parameters (e.g., member sizes, structural properties) and corresponding output responses (maximum inter-story drift ratios), are then assembled into a structured dataset. A detailed flowchart of this dataset generation procedure, from initial design generation to final data assembly for neural network training and testing, is presented in Fig. 6. The flowchart clearly delineates the sequential steps, which include constraint verification, nonlinear time-history analysis, response extraction, and the final partitioning of the dataset into training and testing subsets, with 80% of the data allocated to training and the remaining 20% to testing.

[DOI: 10.22068/ijoce.2026.16.2.665]

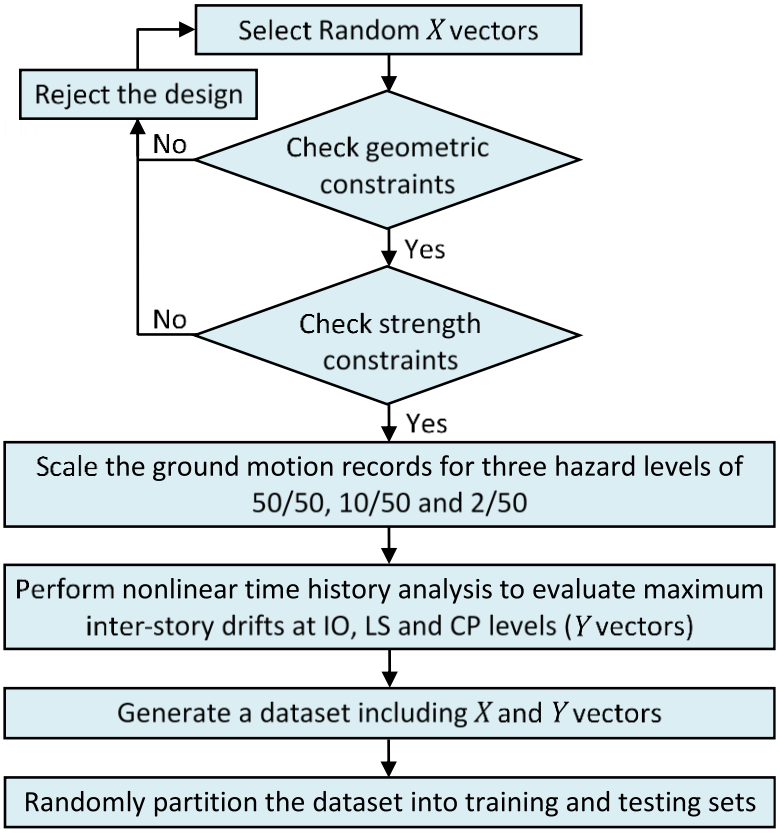

Figure 6: Dataset generation flowchart

The accuracy of the neural network model's predictions is evaluated using three metrics: Mean Absolute Percentage Error (*MAPE*), Root Mean Square Error (*RMSE*), and the Coefficient of Determination (R^2). These metrics are defined as follows:

$$MAPE = \frac{100}{ns}\sum_{i=1}^{ns}\left|\frac{t_i - y_i}{t_i}\right| \tag{10}$$

$$RMSE = \sqrt{\frac{1}{ns}\sum_{i=1}^{ns}(t_i - y_i)^2} \tag{11}$$

$$R^2 = 1 - \frac{\sum_{i=1}^{ns}(t_i - y_i)^2}{\sum_{i=1}^{ns}(t_i - \bar{t})^2} \tag{12}$$

where ns is the number of samples; t_i is the ith target maximum inter-story drift; y_i is ith predicted maximum inter-story drift; and $\bar{t}$ is the mean of target maximum inter-story drift.

To assess the efficiency of the trained CFBP models, the average Mean Absolute Percentage Error (*AMAPE*), average Root Mean Square Error (*ARMSE*), and average R^2 (AR^2) of the predicted inter-story drifts are computed for the IO, LS, and CP performance levels. These calculations are performed for both the training and testing phases, as defined below.

[DOI: 10.22068/ijoce.2026.16.2.665]

$$AMAPE_{d_{PL}} = \frac{\left(MAPE_{d_{PL}}\right)_{training} + \left(MAPE_{d_{PL}}\right)_{testing}}{2} \qquad PL = IO, LS, CP \qquad (13)$$

$$ARMSE_{d_{PL}} = \frac{\left(RMSE_{d_{PL}}\right)_{training} + \left(RMSE_{d_{PL}}\right)_{testing}}{2} \qquad PL = IO, LS, CP \qquad (14)$$

$$AR^2_{d_{PL}} = \frac{\left(R^2_{d_{PL}}\right)_{training} + \left(R^2_{d_{PL}}\right)_{testing}}{2} \qquad PL = IO, LS, CP \qquad (15)$$

For each of the two design examples (the 6-story and 12-story steel MRFs), four distinct CFBP neural network models are developed, differing solely in the number of neurons in their single hidden layer. Specifically, models with 5, 10, 15, and 20 hidden neurons are trained and compared. These configurations are denoted as CFBP5, CFBP10, CFBP15, and CFBP20, respectively. The selected range of hidden neuron counts allows systematic investigation of model complexity versus prediction accuracy, spanning from a relatively small network (CFBP5) to a larger one (CFBP20) that may capture more intricate nonlinear relationships.

5. NUMERICAL EXAMPLES

The dead load of 2500 kg/m and the live load of 1000 kg/m are applied to all beams. The modulus of elasticity and yield stress of materials are E = 210 GPa and F_y = 235 MPa, respectively. The constitutive law is bilinear with a pure strain hardening slope of 3% of the elastic modulus. The sections of beams and columns are selected from the W-shaped sections listed in Table 2.

Table 2: Available W-shaped sections

Columns				Beams			
No.	Profile	No.	Profile	No.	Profile	No.	Profile
1	W14×48	13	W14×257	1	W12×19	13	W21×50
2	W14×53	14	W14×283	2	W12×22	14	W21×57
3	W14×68	15	W14×311	3	W12×35	15	W24×55
4	W14×74	16	W14×342	4	W12×50	16	W21×68
5	W14×82	17	W14×370	5	W18×35	17	W24×62
6	W14×132	18	W14×398	6	W16×45	18	W24×76
7	W14×145	19	W14×426	7	W18×40	19	W24×84
8	W14×159	20	W14×455	8	W16×50	20	W27×94
9	W14×176	21	W14×500	9	W18×46	21	W27×102
10	W14×193	22	W14×550	10	W16×57	22	W27×114
11	W14×211	23	W14×605	11	W18×50	23	W30×108
12	W14×233	24	W14×665	12	W21×44	24	W30×116

5.1 First example: 6-story SMF

A dataset comprising 200 randomly generated samples is used to train and test the neural network models. The components of the output vector are illustrated in Figs. 7 through 9.

[DOI: 10.22068/ijoce.2026.16.2.665]

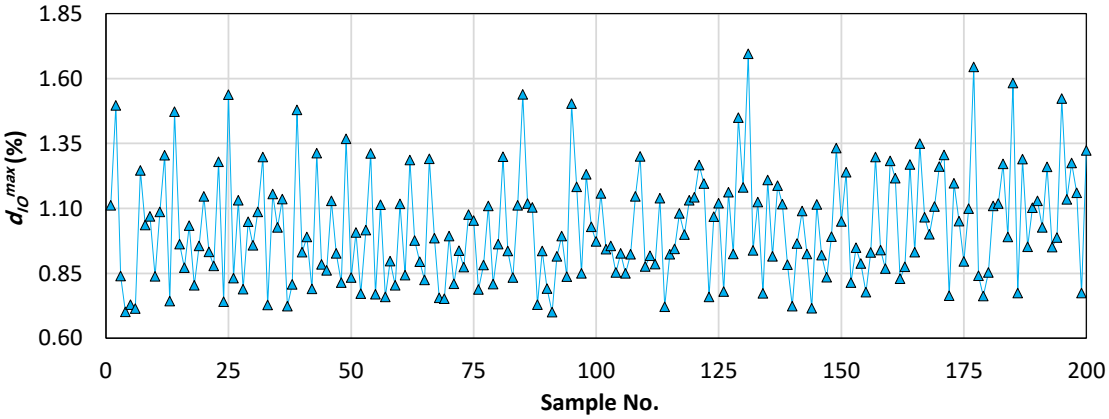

Figure 7: Maximum inter-story drift ratios at the IO level for the 6-story frame

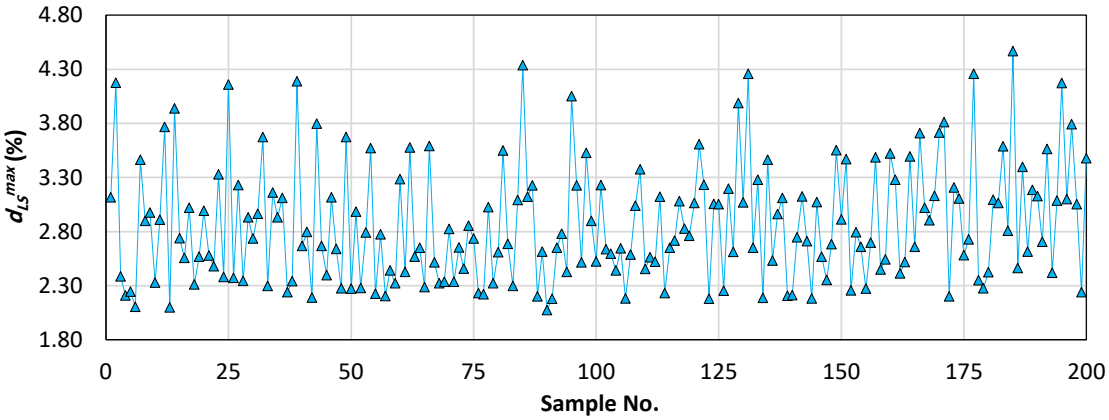

Figure 8: Maximum inter-story drift ratios at the LS level for the 6-story frame

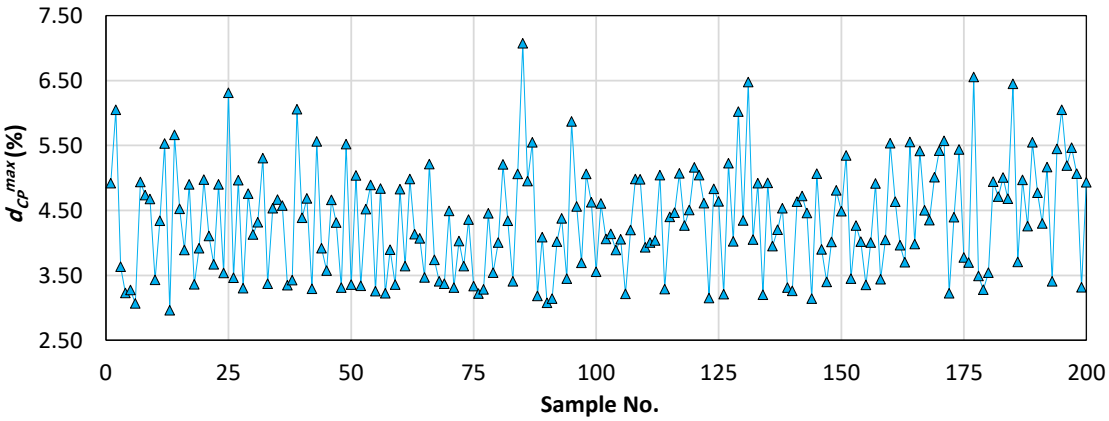

Figure 9: Maximum inter-story drift ratios at the CP level for the 6-story frame

The CFBP5, CFBP10, CFBP15, and CFBP20 neural network models are trained and tested, and their results, expressed in terms of MAPE, RMSE, and R^2, are reported in Tables 3 through 6.

[DOI: 10.22068/ijoce.2026.16.2.665]

Table 3: Performance evaluation of CFBP5 for the 6-story frame

Phase	Metric	Maximum nonlinear time history inter-story drift ratio (%)		
		d_{max}^{IO}	d_{max}^{LS}	d_{max}^{CP}
Training	*MAPE*	3.2526	2.8331	2.5979
	RMSE	0.0429	0.0974	0.1387
	R^2	0.9554	0.9644	0.9711
Testing	*MAPE*	4.6470	4.9253	4.8853
	RMSE	0.0551	0.1733	0.2611
	R^2	0.9467	0.9222	0.9198

Table 4: Performance evaluation of CFBP10 for the 6-story frame

Phase	Metric	Maximum nonlinear time history inter-story drift ratio (%)		
		d_{max}^{IO}	d_{max}^{LS}	d_{max}^{CP}
Training	*MAPE*	2.5517	1.3785	0.6867
	RMSE	0.0350	0.0491	0.0392
	R^2	0.9703	0.9909	0.9976
Testing	*MAPE*	4.6395	5.2945	6.3391
	RMSE	0.0611	0.1775	0.3369
	R^2	0.9345	0.9185	0.8665

Table 5: Performance evaluation of CFBP15 for the 6-story frame

Phase	Metric	Maximum nonlinear time history inter-story drift ratio (%)		
		d_{max}^{IO}	d_{max}^{LS}	d_{max}^{CP}
Training	*MAPE*	2.2532	0.9355	0.3904
	RMSE	0.0299	0.0349	0.0218
	R^2	0.9784	0.9954	0.9993
Testing	*MAPE*	4.0372	4.5960	6.1593
	RMSE	0.0504	0.1727	0.3333
	R^2	0.9556	0.9229	0.8995

Table 6: Performance evaluation of CFBP20 for the 6-story frame

Phase	Metric	Maximum nonlinear time history inter-story drift ratio (%)		
		d_{max}^{IO}	d_{max}^{LS}	d_{max}^{CP}
Training	*MAPE*	1.7928	0.3646	0.1049
	RMSE	0.0226	0.0132	0.0060
	R^2	0.9876	0.9993	0.9999
Testing	*MAPE*	5.7401	7.1013	10.010
	RMSE	0.0833	0.2521	0.5493
	R^2	0.8786	0.8357	0.6454

The *AMAPE*, *ARMSE*, and AR^2 for the predicted inter-story drift ratios at the IO, LS, and CP performance levels are presented in Figs. 10, 11, and 12, respectively.

[DOI: 10.22068/ijoce.2026.16.2.665]

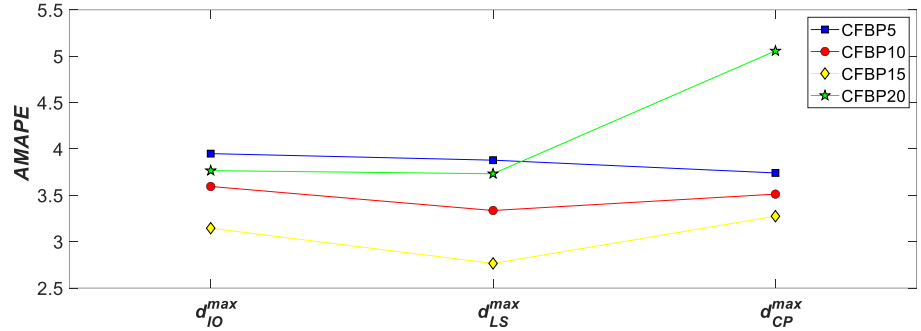

Figure 10: *AMAPE* of predicted inter-story drift ratios for the 6-story frame

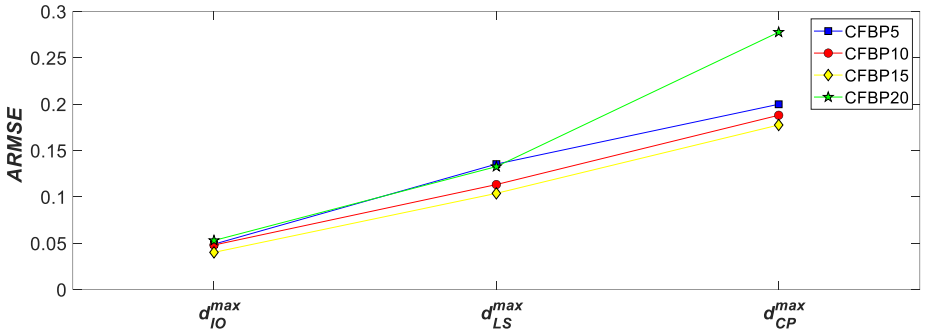

Figure 11: *ARMS*E of predicted inter-story drift ratios for the 6-story frame

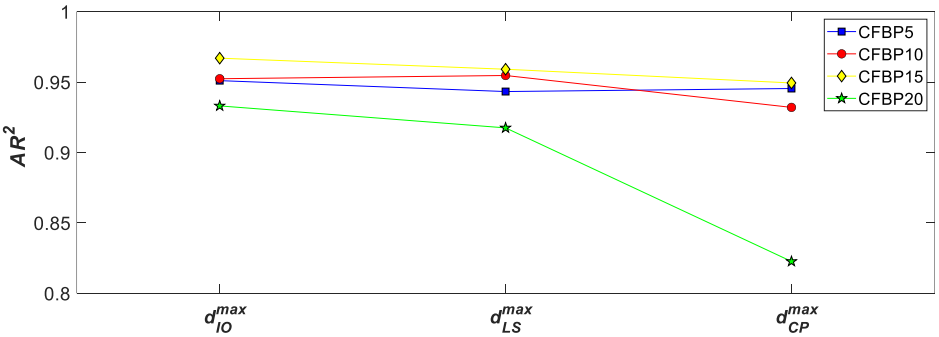

Figure 12: AR^2 of predicted inter-story drift ratios for the 6-story frame

The CFBP15 model consistently outperforms CFBP5, CFBP10, and CFBP20 across all performance levels and evaluation metrics. For *AMAPE*, CFBP15 achieves reductions ranging from 6.77% (vs. CFBP10 at CP) to 35.24% (vs. CFBP20 at CP). The largest *AMAPE* improvements occur at the LS level (28.70% below CFBP5, 17.10% below CFBP10, 25.91% below CFBP20). Similarly, ARMSE reductions vary from 5.58% (vs. CFBP10 at CP) to 36.05% (vs. CFBP20 at CP). Regarding AR^2, CFBP15 yields modest gains over CFBP5 and CFBP10 (0.42%-1.68%) but a substantial 15.41% increase over CFBP20 at the CP level. These results demonstrate that the CFBP model with 15 hidden neurons provides the most accurate predictions of nonlinear time-history inter-story drift ratios at all seismic performance levels.

[DOI: 10.22068/ijoce.2026.16.2.665]

Figs. 13 and 14 display the Absolute Percentage Error (*APE*) of the predicted maximum inter-story drifts, along with the regression results during the training and testing phases for the model with the best prediction accuracy.

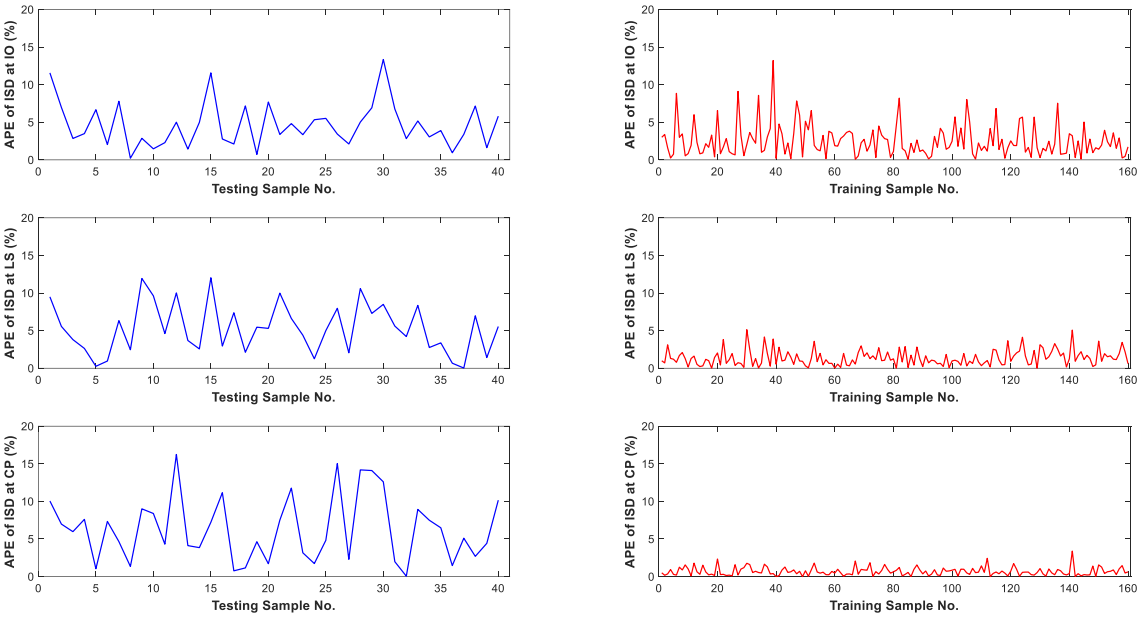

Figure 13: *APE*s of the predicted inter-story drifts using 15 neurons for the 6-story frame

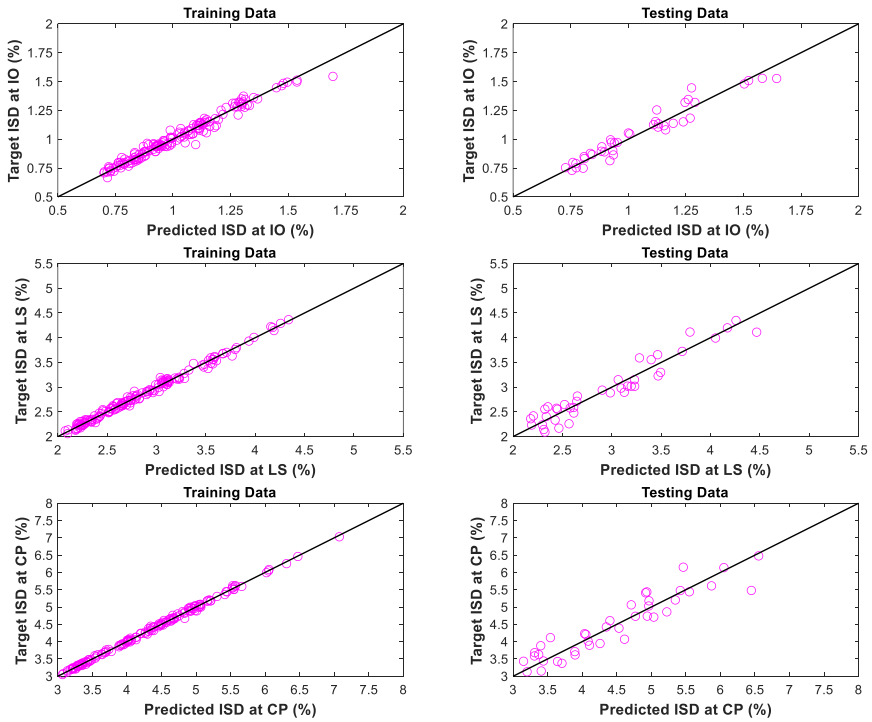

Figure 14: Prediction of inter-story drifts using 15 neurons for the 6-story frame

[DOI: 10.22068/ijoce.2026.16.2.665]

5.2 First example: 12-story SMF

A dataset of 500 randomly generated samples is employed to train and test the NN models, with the output vector components shown in Figs. 15 through 17.

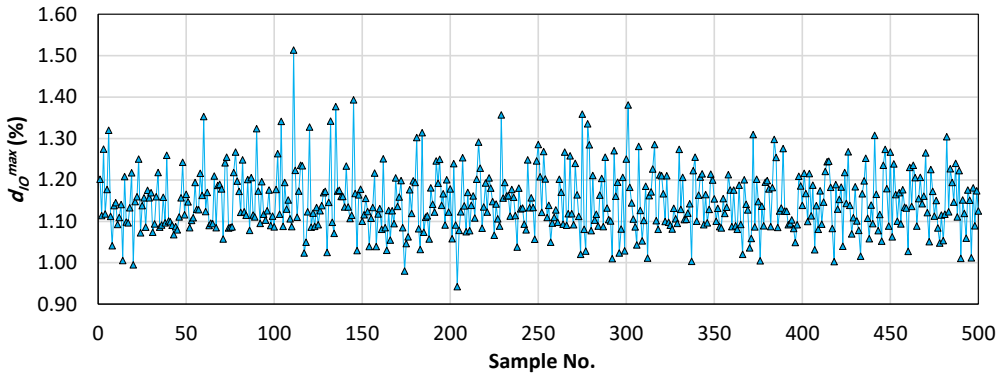

Figure 15: Maximum inter-story drift ratios at the IO level for the 12-story frame

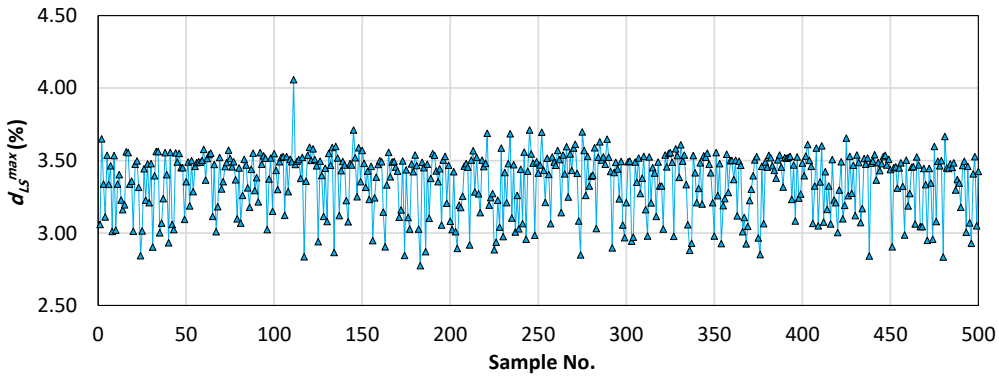

Figure 16: Maximum inter-story drift ratios at the LS level for the 12-story frame

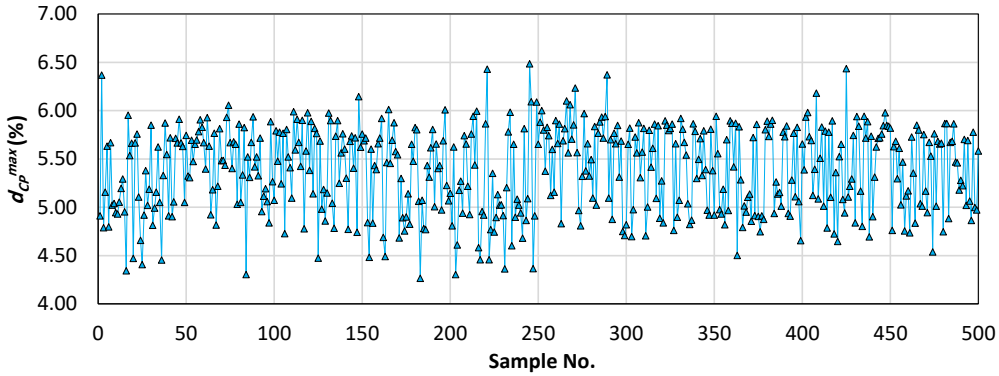

Figure 17: Maximum inter-story drift ratios at the CP level for the 12-story frame

The CFBP5, CFBP10, CFBP15, and CFBP20 neural network models are trained and tested, and their results, expressed in terms of *MAPE*, *RMSE*, and R^2, are reported in Tables 7 through 10.

[DOI: 10.22068/ijoce.2026.16.2.665]

Table 7: Performance evaluation of FFBP5 for the 12-story frame

Phase	Metric	Maximum nonlinear time history inter-story drift ratio (%)		
		d_{max}^{IO}	d_{max}^{LS}	d_{max}^{CP}
Training	*MAPE*	2.3934	2.0863	4.0769
	RMSE	0.0363	0.0962	0.2891
	R^2	0.7809	0.7877	0.5647
Testing	*MAPE*	2.6035	2.3349	4.4393
	RMSE	0.0354	0.0955	0.3230
	R^2	0.6616	0.8053	0.5110

Table 8: Performance evaluation of FFBP10 for the 12-story frame

Phase	Metric	Maximum nonlinear time history inter-story drift ratio (%)		
		d_{max}^{IO}	d_{max}^{LS}	d_{max}^{CP}
Training	*MAPE*	2.2558	2.1163	4.0124
	RMSE	0.0327	0.0976	0.2698
	R^2	0.7697	0.7817	0.5824
Testing	*MAPE*	2.7791	2.3348	4.4255
	RMSE	0.0382	0.0960	0.3233
	R^2	0.6065	0.8033	0.5102

Table 9: Performance evaluation of FFBP15 for the 12-story frame

Phase	Metric	Maximum nonlinear time history inter-story drift ratio (%)		
		d_{max}^{IO}	d_{max}^{LS}	d_{max}^{CP}
Training	*MAPE*	1.2525	0.4550	0.1536
	RMSE	0.0181	0.0193	0.0115
	R^2	0.9453	0.9915	0.9993
Testing	*MAPE*	1.9459	1.7661	3.1059
	RMSE	0.0300	0.0842	0.2202
	R^2	0.7573	0.8487	0.7726

Table 10: Performance evaluation of FFBP20 for the 12-story frame

Phase	Metric	Maximum nonlinear time history inter-story drift ratio (%)		
		d_{max}^{IO}	d_{max}^{LS}	d_{max}^{CP}
Training	*MAPE*	2.2648	2.0616	3.5692
	RMSE	0.0342	0.0956	0.2488
	R^2	0.8054	0.7903	0.6777
Testing	*MAPE*	2.5597	2.3296	3.9141
	RMSE	0.0349	0.0954	0.2800
	R^2	0.6713	0.8057	0.6324

The *AMAPE*, *ARMSE*, and AR^2 for the predicted inter-story drift ratios at the IO, LS, and CP performance levels are presented in Figs. 18 through 20, respectively.

[DOI: 10.22068/ijoce.2026.16.2.665]

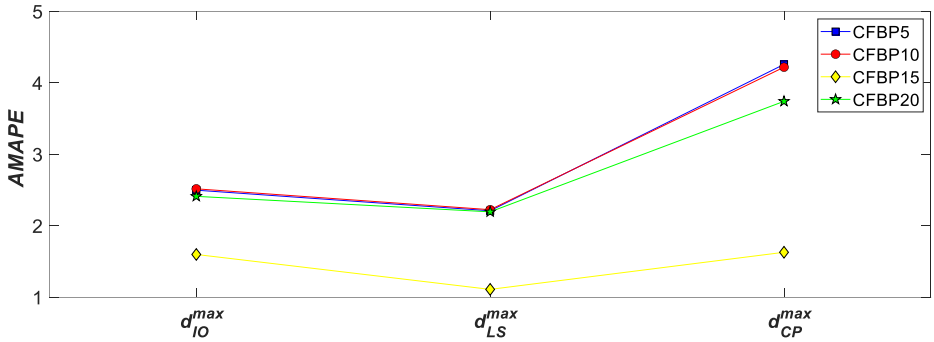

Figure 18: AMAPE of inter-story drift ratios predicted by NN models for the 12-story frame

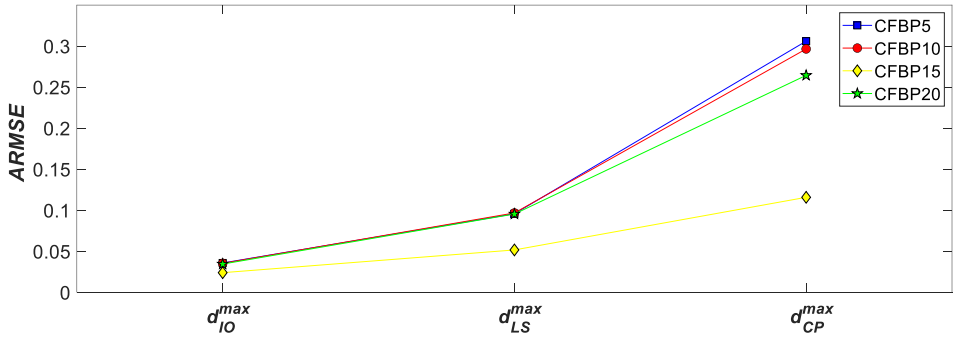

Figure 19: *ARMS*E of inter-story drift ratios predicted by NN models for the 12-story frame

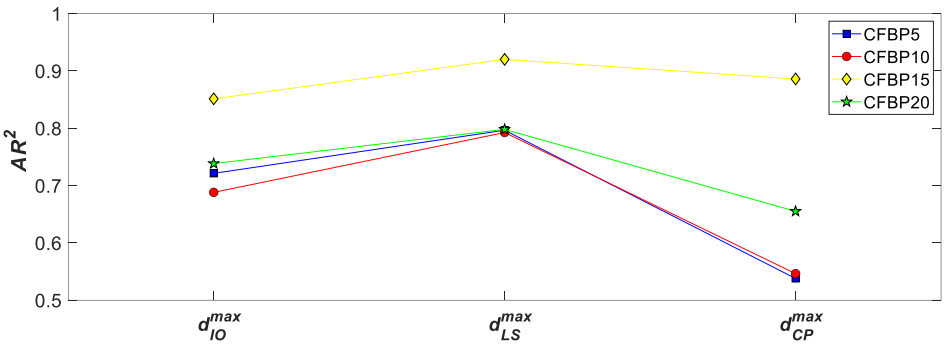

Figure 20: AR^2 of inter-story drift ratios predicted by NN models for the 12-story frame

The CFBP15 model substantially outperforms CFBP5, CFBP10, and CFBP20 across all performance levels. For *AMAPE*, CFBP15 achieves reductions ranging from 33.70% (vs. CFBP20 at IO) to 61.72% (vs. CFBP5 at CP). The largest improvements occur at the CP level, where *AMAPE* is reduced by over 56% relative to all other models. Similarly, *ARMSE* reductions range from 30.39% (vs. CFBP20 at IO) to 62.14% (vs. CFBP5 at CP). Regarding AR^2, CFBP15 yields gains as high as 64.72% (vs. CFBP5 at CP) and 62.17% (vs. CFBP10 at CP), with more modest but still significant increases at IO and LS levels (15-24%). These results conclusively demonstrate that the CFBP neural network model with 15 hidden neurons provides the most accurate predictions of nonlinear time-history inter-story drift ratios at all seismic performance levels.

[DOI: 10.22068/ijoce.2026.16.2.665]

Figs. 21 and 22 display the APE of the predicted maximum inter-story drifts, along with the regression results during the training and testing phases for the model with the best prediction accuracy.

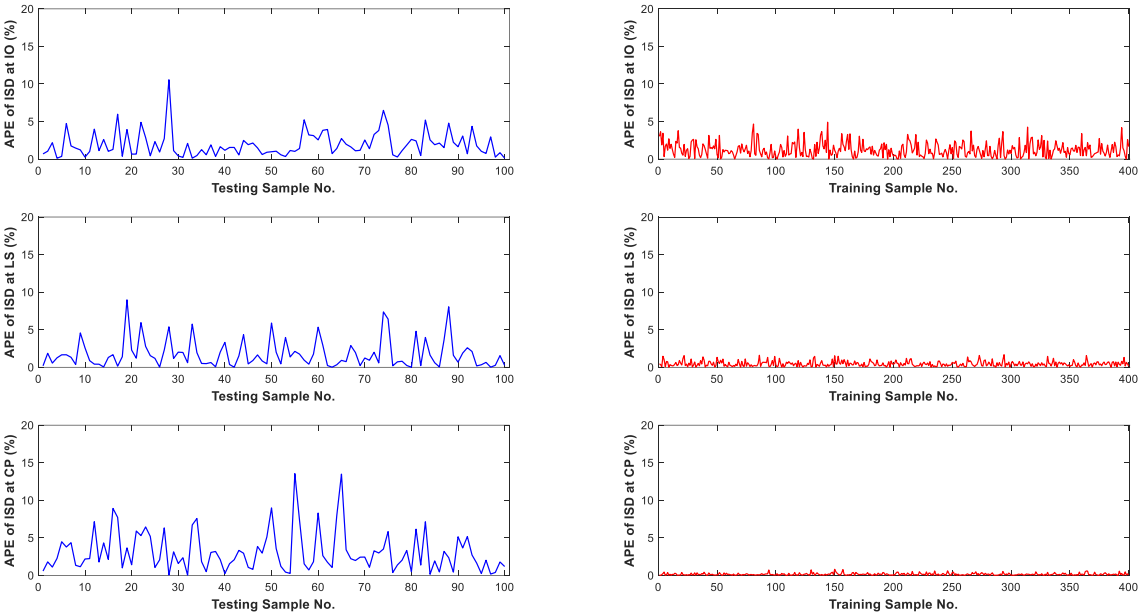

Figure 21: *APE*s of the predicted inter-story drifts using 15 neurons for the 12-story frame

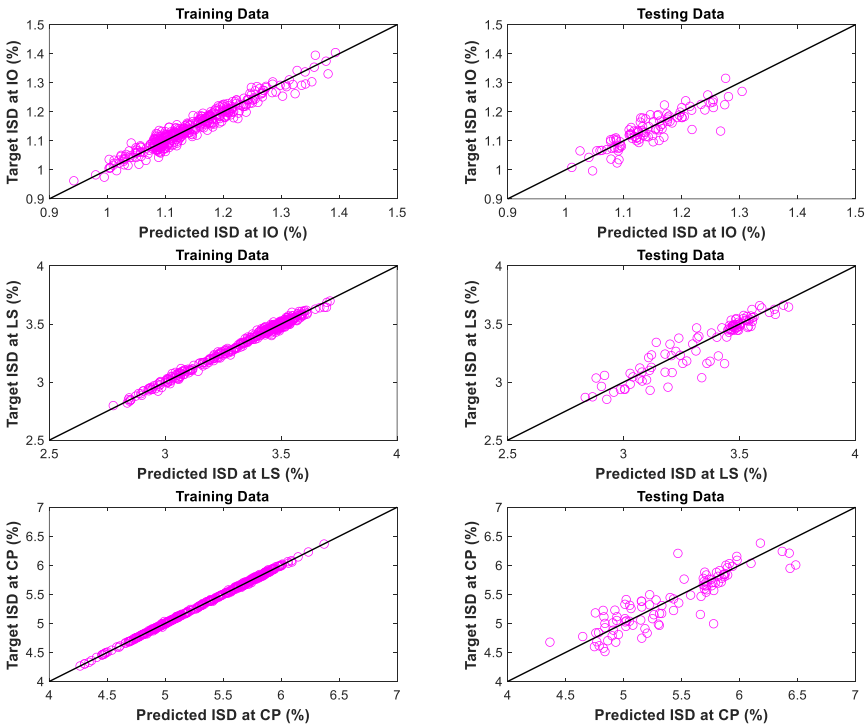

Figure 22: Prediction of inter-story drifts using 15 neurons for the 12-story frame

[DOI: 10.22068/ijoce.2026.16.2.665]

6. CONCLUSIONS

This study investigated the use of cascade-forward back-propagation (CFBP) neural network models to predict the maximum inter-story drift ratios of planar steel moment-resisting frames (MRFs) at three seismic performance levels: immediate occupancy (IO), life safety (LS), and collapse prevention (CP). Two design examples, a 6-story and a 12-story steel MRF, were considered. CFBP models with 5, 10, 15, and 20 hidden layer neurons (denoted CFBP5, CFBP10, CFBP15, and CFBP20) were trained and tested using randomly generated datasets of 200 and 500 samples, respectively. The predictive performance was evaluated using the Mean Absolute Percentage Error (*MAPE*), Root Mean Square Error (*RMSE*), and coefficient of determination (R^2), along with their averaged counterparts (*AMAPE*, *ARMSE*, AR^2). The main findings are summarized as follows:

- For both the 6-story and 12-story frames, the CFBP15 model consistently outperformed CFBP5, CFBP10, and CFBP20 across all performance levels and evaluation metrics. This indicates that a moderate number of hidden neurons (15) provides the best balance between model complexity and generalization capability for this type of seismic response prediction.
- For the 6-story frame, compared to other CFBP architectures, CFBP15 reduced *AMAPE* by up to 35.24% (at CP vs. CFBP20) and *ARMSE* by up to 36.05% (at CP vs. CFBP20). AR^2 improvements were modest against CFBP5 and CFBP10 (0.42%-1.68%) but reached 15.41% at the CP level against CFBP20.
- For the 12-story frame, the superiority of CFBP15 was even more pronounced for the taller frame. *AMAPE* reductions ranged from 33.70% (IO vs. CFBP20) to 61.72% (CP vs. CFBP5). *ARMSE* reductions reached as high as 62.14% (CP vs. CFBP5), and AR^2 gains were substantial, particularly at CP (up to 64.72% over CFBP5).
- The CFBP15 model performed best for both the 6-story and 12-story MRFs, despite the latter exhibiting more complex nonlinear behavior. This consistency suggests that the proposed approach is robust and scalable within the range of low-to-medium-rise steel MRFs.

The trained CFBP15 neural network can serve as an efficient surrogate for computationally expensive nonlinear time-history analyses in performance-based design and optimization frameworks. It enables rapid prediction of maximum inter-story drift ratios at multiple performance levels without repeated dynamic simulations.

REFERENCES

1. FEMA-356, *Prestandard and Commentary for the Seismic Rehabilitation of Buildings*. Federal Emergency Management Agency, Washington DC, 2000.
2. Kaveh A, Zakian P. Performance based optimal seismic design of RC shear walls incorporating soil–structure interaction using CSS algorithm. *Int J Optim Civil Eng* 2012; **2**: 383–405.
3. Liang JC, Li LJ, He JN. Performance-based multi-objective optimum design for steel structures with intelligence algorithms. *Int J Optim Civil Eng* 2015; **5**: 79–101.

[DOI: 10.22068/ijoce.2026.16.2.665]

4. Gholizadeh S. Performance-based optimum seismic design of steel structures by a modified firefly algorithm and a new neural network. *Adv Eng Softw* 2015; **81**: 50–65.
5. Rahami H, Mohebian P, Mousavi M. Performance-based connection topology optimization of unbraced and X-braced steel frames. *Int J Optim Civil Eng* 2017; **7**:451–68.
6. Ganjavi B, Hajirasouliha I. Optimum performance-based design of concentrically braced steel frames subjected to near-fault ground motion excitations. *Int J Optim Civil Eng* 2019; **9**:177–93.
7. Gholizadeh S, Ebadijalal M. Performance based discrete topology optimization of steel braced frames by a new metaheuristic. *Adv Eng Softw* 2018; **123**: 77–92.
8. Kaveh A, Zolghadr A. Topology optimization of trusses considering static and dynamic constraints using the CSS. *Appl Soft Comput*, 2013; **13**: 2727–34.
9. Kaveh A, Javadi SM. Shape and size optimization of trusses with multiple frequency constraints using harmony search and ray optimizer for enhancing the particle swarm optimization algorithm. *Acta Mech*, 2014; **225**: 1595–606.
10. Kaveh A, Mirzaei B, Jafarvand A. An improved magnetic charged system search for optimization of truss structures with continuous and discrete variables. *Appl Soft Comput*, 2015; **28**: 400–10.
11. Kaveh A, Talatahari S. An enhanced charged system search for configuration optimization using the concept of fields of forces. *Struct Multidiscip Optim*, 2011; **43**: 339–51.
12. Kaveh A, Talatahari S. A charged system search with a fly to boundary method for discrete optimum design of truss structures. *Asian J Civil Eng*, 2010; **11**: 277–93.
13. Kaveh A, Bakhshpoori T, Hamze-Ziabari SM. GMDH-based prediction of shear strength of FRP-RC beams with and without stirrups. *Comput Concr* 2018;**22**:197–207.
14. Kaveh A, Eskandari A. Analysis of double-layer barrel vaults using different neural networks; a comparative study. *Int J Optim Civil Eng* 2021;**11**:113-41.
15. Kaveh A, Dadras Eslamlou A, Javadi SM, Geran Malek N. Machine learning regression approaches for predicting the ultimate buckling load of variable-stiffness composite cylinders. Acta Mechanica 2021;**232**:921-31.
16. Kaveh A, Khavaninzadeh N. Efficient training of two ANNs using four meta-heuristic algorithms for predicting the FRP strength. *Structures* 2023;**52**:256–72.
17. Kaveh A, Seddighian MR, Farsi N. A metaheuristic-based artificial neural network for plastic limit analysis of frames. *Int J Optim Civil Eng* 2023;**13**:143-54.
18. Standard No. 2800. Iranian Code of Practice for Seismic Resistant Design of Buildings, Building and Housing Research Center, Tehran, 2014.
19. *OpenSees*. Open System For Earthquake Engineering Simulation. ver 3.3.0 [Computer software]. PEER, Berkeley, CA.
20. Fattahi F, Gholizadeh S. Seismic fragility assessment of optimally designed steel moment frames. *Eng Struct* 2019;**179**:37–51.
21. Gholizadeh S, Danesh M, Gheyratmand C. A new Newton metaheuristic algorithm for discrete performance-based design optimization of steel moment frames. *Comput Struct* 2020;**234**:106250.

[DOI: 10.22068/ijoce.2026.16.2.665]

22. Ghaderi M, Gholizadeh S. Mainshock–aftershock low-cycle fatigue damage evaluation of performance-based optimally designed steel moment frames. *Eng Struct* 2021;**237**:112207.
23. Gholizadeh S, Hasançebi O, Eser H, Koçkaya O. Seismic collapse safety based optimization of steel Moment-Resisting frames. *Structures* 2022;**237**:112207.
24. Hagan MT, Demuth HB, Beal MH. Neural network design, PWS Publishing Company, Boston, 1996.
25. AISC 360-16. Specification for structural steel buildings. Chicago: American Institute of Steel Construction; 2016.

[DOI: 10.22068/ijoce.2026.16.2.665]